Dynamics of Capillary Drying in Water

Kevin Leung,[1] Alenka Luzar,[2] and Dusan Bratko[3]
[1]*Sandia National Laboratories, MS 1421, Albuquerque, New Mexico 87185*
[2]*Department of Pharmaceutical Chemistry, University of California, San Francisco, California 94143*
[3]*College of Chemistry, University of California, Berkeley, California 94720*
(Received 17 July 2002; published 13 February 2003)

We use atomistic simulations to address the question when capillary evaporation of water confined in a hydrocarbonlike slit is kinetically viable. Activation barriers and absolute rates of evaporation are estimated using open ensemble Monte Carlo–umbrella sampling and molecular dynamics simulations. At ambient conditions, the evaporation rate in a water film four molecular diameters thick is found to be of the order $10^5(\mathrm{nm}^2\,\mathrm{s})^{-1}$, meaning that water readily evaporates. Films more than a few nanometers thick will persist in a metastable liquid state. Dissolved atmospheric gas molecules do not significantly decrease the activation barrier.

DOI: 10.1103/PhysRevLett.90.065502 PACS numbers: 61.25.Em, 02.70.Ns, 02.70.Uu, 64.70.Fx

When water is confined between weakly attractive hydrophobic surfaces (contact angles above 90°) and the separation distance is small, it should spontaneously evaporate [1]. Hydrophobic surfaces favor the vapor phase [2], and this surface effect ultimately dominates the liquid phase chemical potential advantage in a sufficiently narrow slit geometry. The large surface tensions and contact angles water can support mean that this dramatic "capillary drying" transition can occur below a critical intersurface distance D_c of order 100 nm [3–5].

Surface force apparatus (SFA) and atomic force microscopy (AFM) experiments regularly study interactions between hydrophobic surfaces immersed in water at intersurface separations *well below* D_c. The metastability of water in these experiments has been inferred from the microscopic bridging vapor cavities observed when the hydrophobic probe surfaces are brought into contact and then pulled apart [6,7]. Because bridging cavities give rise to a long-range attraction [6,8], capillary drying has also been invoked [6–8] as a possible explanation of the anomalous attraction (> 20 nm in range and much stronger than dispersion forces) observed when hydrophobic surfaces approach each other [7].

Kinetically, however, the activation barrier for spontaneous evaporation of water from the slit geometry can be considerable. The pertinent transition state [Fig. 1(b)] is a vapor tube of critical size V_c that connects the two surfaces [9]. The transition state free energy barrier ΔG^c scales as D^2, where D is the intersurface distance. This scaling was first predicted using saddle point approximation estimates [9,10]; the barrier was computed in lattice gas simulations [10–12], which include thermal fluctuations, but it is an open question if coarse-grained models can quantitatively describe water dynamics at microscopic length scales. As the SFA or AFM probes approach each other, they tend to snap into contact, precluding detailed studies of the drying transition at D below several nanometers. Thus the time and length scales over which the drying transition spontaneously occurs are not well characterized [13].

SFA/AFM experiments have also shown that degassing of water confined between hydrophobic surfaces can considerably reduce the range of attraction [7,14]. Dissolved atmospheric gas molecules are expected to accumulate next to hydrophobic surfaces [15] and influence the metastability of confined water. They should further act as a nucleation site for the process of water evaporation. Dissolved gases are thus clearly important to the behavior of and interactions mediated by confined water.

In this Letter we report on dynamics of confinement-induced evaporation of water using atomistic potentials. Our work extends previous coarse-grained studies [9,11,12] to models accurate down to molecular length scales. We use a combination of grand canonical ensemble Monte Carlo (GCMC) and molecular dynamics (MD) simulations to compute the free energy barrier for the

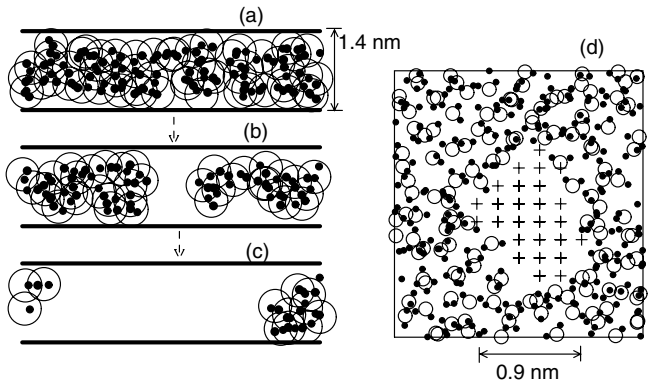

FIG. 1. (a)–(c) Illustration of the capillary drying pathway. The snapshots (cuts are perpendicular to hydrophobic walls) are taken from the umbrella sampling Monte Carlo simulation described in the text. (d) A vapor tubelike transition state configuration (cut is in the plane of the wall); also shown is the lattice grid used to determine the tube or cavity size.

critical vapor tube, ΔG^c, and the rate of capillary drying transition. While there were attempts to use open ensemble simulations to study capillary evaporation in narrow hydrophobic confinements and in equilibrium with bulk water [16–18], we report the first explicit computation of ΔG^c and the absolute rate of evaporation.

The reactive flux formalism [19] is applied. In other words, we (a) choose a "reaction coordinate," in this case the size of the vapor tube/cavity V; (b) compute the free energy profile, $\Delta G(V)$, as V varies, to determine the barrier ΔG^c; (c) compute the "transmission coefficient" κ [19]; and (d) estimate the absolute evaporation rate, k. Steps (a)–(c) are similar to our previous work on lattice gas particles [11,12]. For an isolated vapor tube, the rate, k, of successful barrier crossings is given by

$$k = \kappa(t_p)\langle|\dot{V}(t=0, V=V_c)|/2\rangle\langle\delta(V-V_c)\rangle. \quad (1)$$

$\dot{V} = dV/dt$, V_c is the transition state value of V at which ΔG^c is reached; hence $\langle\delta(V-V_c)\rangle \propto \exp(-\Delta G^c/k_BT)$. $\kappa(t_p) = \langle\dot{V}(t=0, V=V_c)\Theta[V(t_p)-V_c]\rangle/\langle|\dot{V}(t=0, V=V_c)/2|\rangle$ is computed at a "plateau time" t_p [19] chosen sufficiently large that transient dynamics have decayed. Angle brackets represent ensemble averages and Θ is the Heaviside function.

$\Delta G(V)$ is computed using umbrella sampling and GCMC techniques [20], so that the amount of water can spontaneously decrease to accommodate a growing vapor tube. GCMC is performed at $T = 298$ K; for details, see Ref. [18]. We use the simple point charge (SPC) [21] model for water with a smoothed 0.86 nm cutoff [22] of all intermolecular interactions. The excess chemical potential is fixed at $-10.596k_BT$, giving a bulk pressure of 0 ± 10 atm. The water-wall potential mimics water/coarse-grained hydrocarbon Lennard Jones-like interactions [18,22,24]. Our simulations for these potentials yield a contact angle of $135 \pm 5°$, above the experimental value but in agreement with existing theoretical estimates [25]. We consider surface separations of about four molecular diameters (1.4 nm), the width shown to exceed the limit of mechanical instability (spinodal) for a given range of wall-water interaction strength [3,18]. Periodic boundary conditions are applied in the lateral directions. Simulation cells of up to $5.6 \times 5.6 \times 1.4$ nm^3 with up to 1000 water molecules are used. At least 8×10^5 passes are attempted in each umbrella sampling window.

The main challenge of this work lies in measuring V. Since we constrain V in umbrella sampling windows to dynamically accept and reject trial Monte Carlo moves, V must be computed for *all* trials that involve molecules near the cavity. To drastically reduce the computational cost, associated with conventional Voronoi and Delaunay tesselation techniques [23], we measure V by counting connected, unoccupied lattice sites on a cubic lattice with nearest neighbor spacing a. Connectivity is defined in the usual percolation sense, and occupancy means at least one water oxygen lies within $(b + a/2)$ from a site, where b is the effective radius of water molecules. See Fig. 1(d). The δ function in Eq. (1) is then replaced by a Kronecker delta divided by a^3.

The limit $a \to 0$ gives a continuum description of the cavity size and shape. $a = 0.12$ and 0.18 nm are used in this work, and b is 0.17 nm, roughly half the diameter, σ, of a water molecule. Similarly arbitrary choices regarding water size and shape would have to be made if we use the Delaunay technique [23]. While some ambiguities due to discreteness in V cannot be avoided, we note k is strictly an order of magnitude estimate and is not found very sensitive to computational details.

As in Ref. [12], lattice sites do not extend all the way to the walls, but span 0.36 nm ($a = 0.12$ nm) or 0.54 nm ($a = 0.18$ nm) in perpendicular directions. This should not affect ΔG^c because the transition state cavity stretches from one wall to the other, and V is actually a measure of its lateral size. The probability of having the first lattice site unoccupied is the same as finding a spherical void of radius $(a/2 + b)$ in the middle of the metastable liquid. These probabilities are $\sim$1 and 5% for $a = 0.18$ and 0.12 nm, in good agreement with Ref. [26].

Figure 2 shows that ΔG^c values for $a = 0.18$ and 0.12 nm agree well (within $0.8k_BT$) despite a 3.4 times difference in a^3. Henceforth we report ΔG^c as their average, $\simeq 18.7 \pm 1k_BT$. Having shown that our ΔG^c results are converged with respect to a, we use $a = 0.18$ nm unless specified. The transition state at the top of the barrier is a vapor tube with $V_c \simeq 60a^3$ and mean lateral dimension of $\sim$0.8 nm, in fair agreement with mean-field predictions [27]. We stress that the shapes of the tubes are allowed to fluctuate, and many of them are elliptical, not circular. Dipole moments of molecules at the cavity surface are predominantly aligned parallel to the interface, similarly to results for water at a hydrophobic wall [24]. For $D = 1.25$ nm, we find $\Delta G^c \simeq 14.5k_BT$.

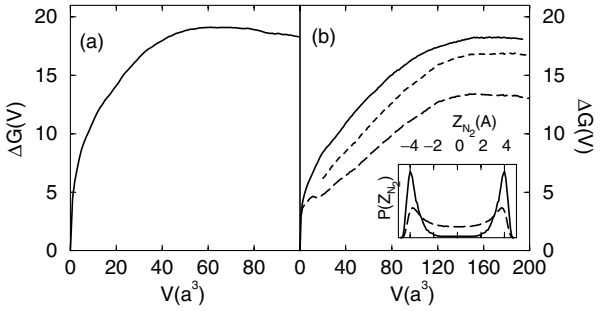

FIG. 2. Free energy [$\Delta G(V)$] profiles as a function of cavity size (V/a^3). (a) $a = 0.18$ nm; (b) $a = 0.12$ nm. Solid lines: pure water; long dashed line: the N_2 molecule is part of cavity; dashed line: translational entropy subtracted from long dashed line (see text). Inset: distribution of the N_2 molecule as a function of the N_2 position Z_{N_2}, in water (solid line) and vacuum (dashed line). Z_{N_2} is the distance between the N_2 center of mass and the midpoint between the walls.

κ in Eq. (1) contributes to the absolute rate and sheds light on the nature of the dynamics. We sample κ using 510 microcanonical MD trajectories, applying the Verlet algorithm and 0.5 fs time steps, starting from 170 successive GCMC configurations at the barrier top taken 10^4 Monte Carlo passes apart. The simulation box has lateral size 8 nm containing up to 2000 molecules. Three sets of initial velocities per configuration, consistent with $T = 298$ K, are randomly generated and propagated. Different configurations appear uncorrelated in their tendencies to reach the evaporated state. To test the system size dependence on $\kappa(t_p)$, we also estimate $\kappa(t_p)$ using 146 trajectories and a simulation cell of lateral size 11.2 nm, containing up to 4000 molecules.

Figure 3 shows that, after a transient of ~10–20 ps, a plateau value of $\kappa = 0.08 \pm 0.03$ is reached. A few representative trajectories that start at $\sim V_c$ are shown in the inset in Fig. 3. Some of them recross the transition state many times and thus exhibit "diffusive behavior," leading to loss of correlation with the inital velocity and, ultimately, a small $\kappa(t_p)$. To put this in perspective, for a related process with many recrossings, namely, the nucleation and condensation of a Lennard Jones liquid from the vapor phase, κ was found to be ~0.003 [28]. Figure 3 also depicts $\kappa(t)$ for the ~4000 molecule cell where $\kappa(t_p) \sim 0.06$. This estimate is based on 4 times fewer trajectories compared to the smaller system and is subject to larger statistical uncertainties. Nevertheless, it indicates a satisfactory convergence with system size. We use $\kappa(t_p)$ only as an order of magnitude estimate.

The "transition state rate," $\langle|\dot{V}(t = 0, V = V_c)/2|\rangle$ in Eq. (1), is found to be $0.082a^3$ fs^{-1}. From Eq. (1), the absolute rate of evaporation via formation of an isolated

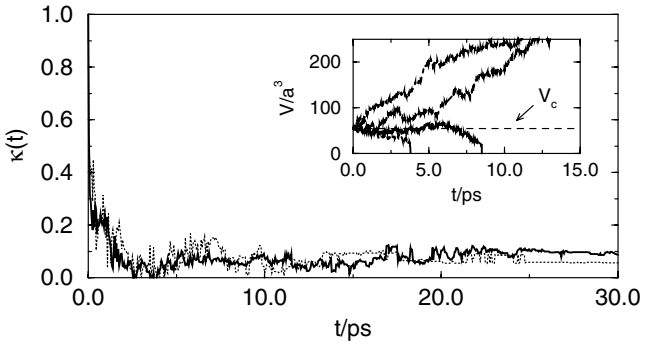

FIG. 3. Transmission coefficient κ as function of time, averaged over 510 trajectories for the ~2000 molecule system (thick solid line), or over 146 trajectories for the ~4000 molecule system (dotted line). Inset: four typical trajectories characterized by the cavity volume as a function of time, all for initial $V \sim V_c$. Some of the trajectories rapidly relax to either $V = 0$ or $V \sim 300a^3$–$600a^3$ (the latter corresponding to vapor tubes up to 2.5 nm diameter). A few (not shown) oscillate in the transition state region, $40a^3 < V < 120a^3$, for up to 50 ps.

critical vapor tube is then $k \approx 0.082\kappa e^{-18.7}$ fs^{-1}, or 5×10^4 s^{-1}. This gives a rate per unit area $\sim 1 \times 10^5$(nm^2 s)$^{-1}$ [assuming a somewhat arbitary (0.7 nm)^2 uncorrelated area for spontaneous fluctuations, where 0.7 nm is less than two correlation lengths in ambient water]. To estimate a rate for an SFA/AFM-like setting with a micron-sized contact area, we find a tube formation rate of 1×10^{11} s^{-1}. Hence evaporation should be fast for $D = 1.4$ nm. Assuming that ΔG^c scales as $(D - \sigma)^2$, where $D - \sigma$ is the slit width accessible to water molecules, and that we have reached the scaling regime, $D = 2.4$ nm will yield a rate of 1.3×10^{-11} s^{-1} for the same contact area, or too slow to be observed over laboratory time scales. The first assumption follows from a saddle point approach [9] and was corroborated by simulations for a coarse-grained model [29]. The second assumption is questionable, but it allows a rough time scale estimate. For large D, overcoming the barrier always represents the rate limiting step [27]. In very thin slits where ΔG^c is low, on the other hand, evaporation time may also depend on the rate of liquid expulsion which can become comparatively slow with increasing lateral size.

To independently corroborate the rate computed using Eq. (1), we have conducted direct microcanonical ensemble MD simulations of evaporation for $D = 1.25$ nm, starting from a metastable liquid film with no vapor tube present. The details are otherwise similar to those used in sampling κ. On the average, a vapor tube spontaneously forms in 0.8 ± 0.1 ns. Assuming the prefactors are the same as for $D = 1.4$ nm, the directly simulated evaporation rate is comparable to the absolute rate predicted by Eq. (1).

Finally, we examine the effect of an isolated N_2 on ΔG^c for evaporation of confined water. We ensure that N_2 is part of the simulated vapor tube by tagging one unoccupied lattice site in the middle of the slit to its lateral position. Using the N_2 force fields of Ref. [30] and $a = 0.12$ nm yields $\Delta G^c \sim 13.4k_BT$ for $D = 1.4$ nm when N_2 is in the vapor tube [Fig. 2(b)], seemingly reducing ΔG^c by $\sim 5.4k_BT$. This large difference is misleading and is partly due to the translational entropy of N_2 (an internal degree of freedom) within the cavity. Subtracting this translational entropy of N_2 [see dashed line in Fig. 2(b)] yields the correct N_2-related decrease in ΔG^c of just $2.0k_BT$. The effect is $1.6k_BT$ smaller than the predicted free energy release upon moving N_2 from bulk water to vacuum [30]. The reason is that N_2 is in a nonbulk environment; the inset of Fig. 2(b) shows N_2 in the presence of water to be strongly attracted to the hydrophobic surfaces. Assuming the midpoint density in the $D = 1.4$ nm slit is close to the bulk one, the overall N_2 concentration in the slit is found to be an order of magnitude higher than in bulk water. Both effects, N_2 reducing ΔG^c and the adsorption of N_2, make it more likely the tube will initiate in the vicinity of N_2.

Nevertheless, the saturated concentration of bulk phase N_2 close to 0.6 mM may not suffice to significantly affect the evaporation rate. At this low concentration, the reduction in ΔG^c cannot outweigh the penalty for the tube localization at N_2. We have confirmed this in direct microcanonical ensemble evaporation simulation runs. N_2 adsorption indicated by the distribution profile shown in Fig. 2(b) may, however, increase the gas concentration in the confinement affecting both the mechanism and the overall rate of the tube formation. In future work, we intend to address these issues using an ensemble open to N_2 molecules to mimic an equilibrium with bulk N_2 solution.

In conclusion, we have introduced an efficient algorithm for simulating thermodynamic and kinetic properties of cavities in confined water. The capillary evaporation activation barrier for a 1.4 nm thick layer of water is $\sim 18.7 k_B T$ for a water-hydrocarbon potential. We find that a cavity volume reaction coordinate is adequate to treat water at ~ 1 nm length scales. For a micron-sized contact area, we find that evaporation should proceed in a subnanosecond time scale. A pure water layer twice as thick (or more) will remain metastable over laboratory time scales. The directly simulated evaporation rate for $D = 1.25$ nm is consistent with our ΔG^c estimate. While N_2 molecules lower ΔG^c of vapor tubes in their vicinity, their equilibrium concentration is too small to change the rate of capillary evaporation. This leaves open the question of whether apparent nonequilibrium effects, such as air nanobubbles recently found on hydrophobic surfaces [31] or quenched surface defects such as hydrocarbon protrusion from the surface, increase the evaporation rate in experimental settings. The implications to nanoscience [17] and to biological systems [32] are also potentially intriguing. Our methods should be amenable to examining these issues in the future.

We thank Daan Frenkel, Paul Madden, Hugo Christenson, Amalie Frischknecht, Aidun Thompson, Stjepan Marčelja, and José Teixeira for helpful discussions. This work was supported by DOE under Contract No. DE-AC04-94AL85000 to Sandia National Laboratories (K. L.) and NSF Grants No. CHE-0211626 (A. L.) and No. BES-0118208 (D. B.). Partial support from NSF-NCSA under CHE010023N (A. L.) for the supercomputer time is also acknowledged.

[1] J. N. Israelachvili, *Intermolecular and Surface Forces* (Academic, London, 1992).
[2] F. H. Stillinger, J. Solution Chem. **2**, 141 (1973).
[3] T. M. Truskett *et al.*, J. Chem. Phys. **114**, 2401 (2001).
[4] K. Lum and A. Luzar, Phys. Rev. E **56**, R6283 (1997).
[5] K. Lum *et al.*, J. Phys. Chem. B **103**, 4570 (1999).
[6] H. K. Christenson and P. M. Claesson, Science **239**, 390 (1988); J. L. Parker *et al.*, J. Phys. Chem. **98**, 8468 (1994).
[7] For a review, see H. K. Christenson and P. M. Claesson, Adv. Colloid Interface Sci. **91**, 391 (2001).
[8] D. R. Berard *et al.*, J. Chem. Phys. **98**, 7236 (1993).
[9] V. S. Yushchenko *et al.*, J. Colloid Interface Sci. **96**, 307 (1983).
[10] See F. Restagno *et al.*, Phys. Rev. Lett. **84**, 2433 (2000) for the closely related problem of capillary condensation.
[11] A. Luzar and K. Leung, J. Chem. Phys. **113**, 5836 (2000).
[12] K. Leung and A. Luzar, J. Chem. Phys. **113**, 5845 (2000).
[13] Dynamic force measurements have been proposed to study this process: O. I. Vinogradova and R. G. Horn, Langmuir **17**, 1604 (2001); J. N. Israelachvili (personal communication).
[14] V. S. J. Craig *et al.*, Langmuir **15**, 1562 (1999); R. F. Considine *et al.*, Langmuir **15**, 1657 (1999).
[15] D. Beaglehole, J. Phys. Chem. **91**, 5091 (1987); M. Alfridsson *et al.*, Langmuir **16**, 10087 (2000).
[16] A. Luzar *et al.*, J. Chem. Phys. **86**, 2955 (1987); A. Wallqvist and B. J. Berne, J. Phys. Chem. **99**, 2893 (1995); J. Forsman *et al.*, J. Phys. Chem. B **101**, 4253 (1997); I. V. Brovchenko *et al.*, Fluid Phase Equilib. **183**, 331 (2001); E. N. Brodskaya *et al.*, Langmuir **17**, 4443 (2001); T. Hayashi *et al.*, J. Chem. Phys. **117**, 6271 (2002).
[17] G. Hummer *et al.*, Nature (London) **414**, 188 (2001).
[18] D. Bratko *et al.*, J. Chem. Phys. **115**, 3873 (2001).
[19] C. H. Bennett, in *Algorithms for Chemical Computations*, edited by R. E. Christofferson (American Chemical Society, Washington, D.C., 1977); D. Chandler, J. Chem. Phys. **68**, 2959 (1978).
[20] D. Frenkel and B. Smit, *Understanding Molecular Simulation: From Algorithms to Applications* (Academic, New York, 1996).
[21] H. J. C. Berendsen *et al.*, in *Intermolecular Forces*, edited by B. Pullman (Reidel, Dordrecht, 1981), p. 331.
[22] J. C. Shelley and G. N. Patey, Mol. Phys. **88**, 385 (1996), which also gave the rationale for our specified cutoffs. Limited trial simulations with 2D [18] and 3D [22] Ewald sums did not appreciably differ from cutoff calculations.
[23] S. Sastry *et al.*, Phys. Rev. E **56**, 5524 (1997); D. R. Barker *et al.*, Phys. Rev. E **62**, 1427 (2000).
[24] C. Y. Lee *et al.*, J. Chem. Phys. **80**, 4448 (1984).
[25] J. Hautman and M. L. Klein, Phys. Rev. Lett. **67**, 1763 (1991).
[26] R. D. Mountain, J. Chem. Phys. **110**, 2109 (1999).
[27] V. V. Yaminsky *et al.*, *Handbook of Surfaces and Interfaces of Materials*, edited by H. S. Nalwa (Academic, New York, 2000), Vol. 4.
[28] P. R. ten Wolde and D. Frenkel, J. Chem. Phys. **109**, 9901 (1998); P. R. ten Wolde *et al.*, J. Chem. Phys. **110**, 1591 (1999).
[29] K. Leung and A. Luzar (to be published).
[30] T. Somasundaram *et al.*, Phys. Chem. Chem. Phys. **1**, 143 (1999); SPC/E water is used in this work.
[31] N. Ishida *et al.*, Langmuir **16**, 6377 (2000); J. W. G. Tyrrell and P. Attard, Phys. Rev. Lett. **87**, 176104 (2001).
[32] G. Hummer *et al.*, Chem. Phys. **258**, 349 (2000); J. D. Weeks, Annu. Rev. Phys. Chem. **53**, 533 (2002).